PCCP

RSC Publishing

PAPER

View Article Online
View Journal | View Issue

Cite this: *Phys. Chem. Chem. Phys.*, 2013, **15**, 6651

QM/MM simulations of vibrational spectra of bacteriorhodopsin and channelrhodopsin-2†

Kai Welke,[a] Hiroshi C. Watanabe,[a] Tino Wolter,[a] Michael Gaus[ab] and Marcus Elstner*[a]

Received 22nd November 2012,
Accepted 17th January 2013

DOI: 10.1039/c3cp44181d

www.rsc.org/pccp

Channelrhodopsin-2 is a light-gated ion channel, which has been studied intensively over the last decade. Vibrational spectroscopic experiments started to shed light on the structural changes, that occur during the photocycle, especially in the hydrogen-bonded network surrounding the protonated D156 and C128 – the DC gate. However, the interpretation of these experiments was only based on homology models. Since then, an X-ray structure and better computational models became available. In this article, we show that in combination with a recent reparametrization, the approximate DFT method, DFTB, is able to describe the effects of hydrogen bonding on the C=O stretch vibration in carboxylic acids reliably and agrees well with full DFT results. We apply DFTB in a QM/MM framework to perform vibrational analysis of buried aspartic acids in bacteriorhodopsin and channelrhodopsin-2. Using this approach, we can simulate the FTIR spectral difference between D115 in the dark-adapted and K states of bacteriorhodopsin. The FTIR experiments on the DC gate in channelrhodopsin-2 are well described using an indirect model, where D156 and C128 are bridged *via* a water molecule.

1 Introduction

Vibrational spectroscopy is a showcase example of simulations and experiments going hand in hand to examine structure, dynamics and function of biomolecules. The spectroscopic experiments provide necessary information for the improvement of simulations, *e.g.* on protonation states of titrable amino acids, conformation of co-factors, *etc.* while the interpretation of these experiments needs models as a connection between observation and structural foundation.

This approach has proven to be especially fruitful in the case of retinal proteins, since changes in the protein structure along the functional cycle of these proteins can be captured elegantly with difference or time-resolved Fourier Transform Infrared (FTIR) Spectroscopy experiments, as exemplified by the work on bacteriorhodopsin (BR).[1–3]

This technique is especially suited to detect changes in protonation states of glutamic or aspartic acids, since first, the position of the ν_{COOH} band (1710–1760 cm^{-1}) is generally free from overlap with those of other residues and is well distinguishable from the symmetric and antisymmetric bands of the unprotonated species (1400–1570 cm^{-1}). Second, the ν_{COOH} band has one of the highest intensities among those in the mid-IR region. Third, the position and shape of the ν_{COOH} band reacts sensitively to changes in the local environment, such as hydrogen-bonding interactions or the local electric field, which acts to stabilize or destabilize the C=O electric dipole moment.[4–6]

Bacteriorhodopsin is a microbial rhodopsin that acts as a proton pump in halobacteria and undergoes a photocycle where the isomerization of the retinal triggers several proton transfer steps. The first intermediate, that can be trapped at low temperatures and is resolved by X-ray experiments, is called "K" (PDB code: 1m0k).[7,8] BR has been studied intensively and is therefore often used as a reference model for QM/MM simulations.[9–14] The difference between the dark-adapted state and the K intermediate was also characterized by FTIR spectroscopy,[15] which showed that D115, a protonated carboxylic acid near the retinal, undergoes changes in its hydrogen-bonded network.

Channelrhodopsin-2 (ChR2) is the best examined representative of the channelrhodopsins,[16] which combines the functions of a photoreceptor and an ion channel into a single protein – a feature, which has not been found before. In its native organism, the unicellular green alga *Chlamydomonas reinhardtii*, the light-induced

[a] *Karlsruhe Institute of Technology, Institute of Physical Chemistry, Kaiserstraße 12, Karlsruhe, Germany. E-mail: marcus.elstner@kit.edu; Fax: +49 721 608 45710; Tel: +49 721 608 45700*

[b] *Theoretical Chemistry Institute, University of Wisconsin-Madison, 1101 University Avenue, Madison, Wisconsin 53706, USA*

† Electronic supplementary information (ESI) available: Detailed benchmark of DFTB performance with respect to DFT. See DOI: 10.1039/c3cp44181d

influx of cations leads to a depolarization of the cell membrane, which causes a change in the motion pattern in response to the light conditions (phototaxis and photophobic behavior). Due to its kinetic properties and good expression levels in host cells, it has been applied in a variety of optogenetic experiments in the neuroscientific field.[17–19]

A series of experiments led to the discovery of a pair of residues, D156 and C128, which is involved in the channeling mechanism in ChR2.[20–24] Replacement of each of these residues led to 100 to 1000-fold longer open states, which is desirable for optogenetic applications. These experiments were interpreted on the basis of homology models, using either sensory rhodopsin II (SRII)[24] or BR as templates,[23] since at that time a crystal structure or a more sophisticated computational model was not available. Due to the homology of ChR2 to other microbial rhodopsins, a direct hydrogen bond between D156 and C128 was proposed, which was termed the "DC gate".[24]

However, the direct model for the DC gate does not fit to some experimental observations. First, in the X-ray structure of the ChR1–ChR2 hybrid (PDB code: 3ug9), the side chain of C128 is oriented away from D156, so that the distance between the sulfur atom of C128 and the nearest oxygen atom of D156 is as large as 4.4 Å.[25] This has also been confirmed in molecular dynamics (MD) studies based on a homology model of ChR2.[26] Next, the simulations show that there is a strongly bonded water molecule between D156 and C128, which stays stable during extended MD simulations.[26] Finally, in the FTIR difference spectrum between the ground state and the first photointermediate P_1, a symmetric band at 1735(−)/1742(+) cm^{-1}‡ was assigned to changes in the hydrogen bonding of D156, although the intensity of the band suggested the involvement of other residues or proton transfer events as well.[22,24] Hydrogen bonds involving sulfur are normally weaker than their oxygen counterparts, so that frequencies for –SH bonded carboxylic acids are expected in the range of 1745–1760 cm^{-1}.[27] In the case of the direct DC gate model, 1735 cm^{-1} would be an example of an exceptionally strong hydrogen bond with sulfur, stronger than the –OH···O hydrogen bond observed for the C128T mutant (1740(+)/1747(−) cm^{-1}) and of similar strength to that observed in the difference spectrum of the K intermediate of BR with respect to a wild type (1733(+)/1740(−) cm^{-1}).[15]

Although the sequence homology between ChR2 and SRII or BR is given for D156 (D115 in BR) and C128 (T90 in BR), issues, such as the relative orientations of the side chains and the role of internal water molecules, cannot be solved by homology modeling. We proposed a refined model for ChR2,[26,28] which provides much greater details and also agrees well with the crystal structure of the ChR1–ChR2 hybrid. Based on this model, we propose that D156 and C128 are bonded *via* a water molecule instead of a direct connection. We show that this model also agrees well with the FTIR experiments and additionally accounts for the additional information provided by the X-ray experiment.

‡ A negative band corresponds to the dark state, while a positive band indicates a band of the intermediate.

The DFT-based approximated method "self-consistent charge density functional tight-binding"[29] (SCC-DFTB or DFTB2) and its extension to third order (DFTB3)[30,31] have already been applied successfully in vibrational spectroscopic studies in hydrogen-bonded systems, both on its own[32] and in a QM/MM framework.[12,13,33] Calculations on rhodopsin models clarified the protonation state of E181. In order to explain the FTIR observations, E181 has to be unprotonated.[33] By analyzing diverse spectroscopic data, including FTIR, simulations of the O intermediate of BR resolved the number of water molecules in the active site to be three at this stage of the photocycle.[13]

However, these studies revealed that the effect of hydrogen bonding on the ν_{COOH} band was overestimated with DFTB2 compared to full DFT in strongly hydrogen-bonded systems, *e.g.* an acetic acid dimer.[12,33] Furthermore, despite the improvements of DFTB3 over DFTB2 with respect to hydrogen binding energies, proton affinities and proton transfer barriers,[31] due to shortcomings of the old "mio" parameters in the description of hydrogen bonds, the performance of the DFTB3–mio combination is inferior to DFTB2 in terms of vibrational frequencies. In this work we show that a recent reparametrization of DFTB: the 3ob parameter set,[34] improves the description of hydrogen-bonded carboxylic acids in proteins.

We first perform normal mode analyses on small hydrogen-bonded clusters of propionic acid and methanol to estimate the effect of hydrogen bonding on the ν_{COOH} band, and show that DFTB3 can describe this effect as reliably as DFT. Then, we compare the difference FTIR spectrum of dark-adapted *vs.* K states of BR. We show that DFTB is able to describe the experimentally observed red-shift from BR to K, which results from subtle structural changes. Finally, we apply the same approach to the ground state of ChR2 and its C128T mutant to propose an indirect model for the DC gate structural motif, which agrees with both the FTIR and the X-ray experiments.

2 Methods

2.1 Calculations on gas phase models

All models for the gas phase calculations were constructed with Avogadro.[35] Normal mode analyses were carried out after geometry optimization with DFTB2/mio[29] (SCC-DFTB), DFTB3/mio[31] or DFTB3/3ob.[34] The tests of a special parametrization for vibrational frequencies, which is labelled "3ob-f",[34] are documented in the ESI.† These calculations were done with a stand-alone implementation of DFTB3.

Density functional calculations were performed with ORCA[36] using the PBE exchange–correlation functional[37] and the def2-TZVP basis and coulomb fitting basis sets.[38,39] Hybrid DFT calculations were performed with PBE0,[40] applying the RIJCOSX approximation[41] in combination with a suitable auxiliary basis.[42] Double hybrid calculations were carried out with the B2PLYP functional[43] with the invocation of the "resolution of the identity" (RI) approximation on the MP2 part[44,45] with a suitable auxiliary basis set[46] and the RIJCOSX approximation on the SCF part. Additional functionals and basis sets were tested, which are documented in the ESI.† All computed

frequencies reported in this work are unscaled harmonic frequencies.

2.2 QM/MM calculations on bacteriorhodopsin

All QM/MM calculations were carried out with DFTB/CHARMM (version c37b1)[47,48] with the mio or 3ob parameter set for the QM region, and the CHARMM22 force field for the rest of the protein.[49,50] The structure for the dark-adapted state was prepared as in a previous study,[14] based on an X-ray structure of 1.55 Å resolution (PDB code: 1c3w).[51] The K intermediate was modeled accordingly, based on the crystal structure of 1.43 Å resolution (PDB code: 1m0k).[8] Standard protonation states were assumed for all titrable residues, except for D115, D96 and E204, which are known to be protonated in both states.[52,53] No restraints were applied during geometry optimization. The QM/MM boundary was chosen to be between the C_α and C_β atoms, using a standard link atom approach. The ''divided frontier'' scheme was applied for the charges of the MM boundary atoms.[54] The normal mode analyses were carried out with the VIBRAN module of CHARMM in a reduced basis, consisting of a single aspartic acid side chain (D115 in BR, D156 in ChR2).

2.3 QM/MM calculations on channelrhodopsin-2

As a model for channelrhodopsin-2, a snapshot obtained from a MD trajectory of a previous study was used.[26,28] These simulations are based on a homology model of ChR2 with the X-ray structure of the ChR1–ChR2 hybrid[25] as a template structure. For the vibrational analysis, only a monomer of the protein and all water molecules within 3 Å of any atom of that monomer were considered. D156, E90 and H201 were modeled protonated.[26] Since the starting structure is an MD snapshot obtained with a classical force field, more residues need to be included in the QM region. Here, the retinal and K257, E162, D252, K58, and 5 closest water molecules in the active site were used in all geometry optimizations on the ChR2 and the C128T mutant in addition to the residues of the DC gate D156 and C128/T128, so that the QM region for ChR2 amounts to 129 atoms. The further procedure and setup were the same as for BR. The C128T mutant was created by simply changing the residue from cysteine to threonine and re-optimizing the structure.

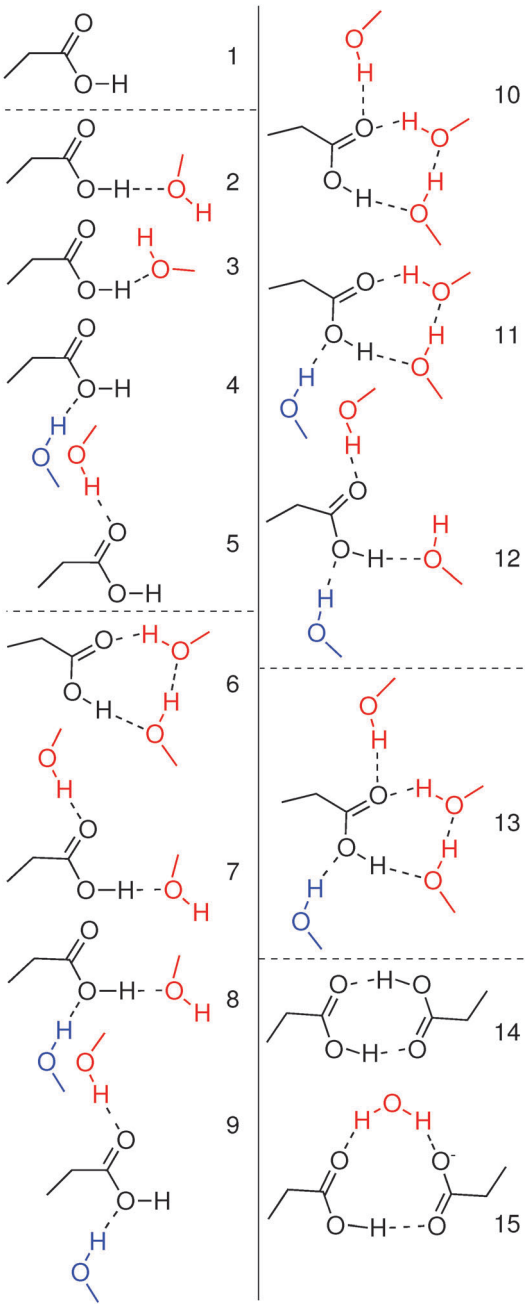

Fig. 1 Gas-phase models of propionic acid and methanol, hydrogen-bonded in different conformations. Molecules in red lower the C=O stretch frequency, while molecules in blue cause blue-shifts.

3 Results and discussion

3.1 Effect of hydrogen bonds on the C=O stretch vibration in the gas phase

At first, we calculated the ν_{COOH} frequencies of several hydrogen-bonded clusters of propionic acid and methanol (Fig. 1) by means of normal mode analysis. By comparing the frequencies of the clusters to the frequency of the free propionic acid (model 1), we are able to examine the effect of one or several hydrogen bonds on the ν_{COOH} band. This could be regarded as simple models for the interaction of aspartic or glutamic acid side chains with serine, threonine or water molecules, although the results are not directly transferable into the protein, since steric influence may prevent optimal hydrogen-bonding geometries, and the electrostatic environment may additionally influence the C=O dipole and therefore the ν_{COOH} band. We have chosen propionic acid as a model for the aspartic acid side chain, since its spectroscopic behavior, *e.g.* the solvent shifts, fits better to side chains in proteins and model peptides than acetic acid.[6]

To judge the performance of DFTB with respect to both absolute values for ν_{COOH} and shifts of the ν_{COOH} band, a proper reference method needs to be chosen. Since DFTB is derived from DFT, a pure DFT exchange–correlation functional is the

natural choice. The popular functionals of the GGA type (generalized gradient approximation) compute harmonic frequencies to similar accuracy, and are overall closer to the experimental frequencies than hybrid GGA functionals,[55] which we also tested for the gas phase models (see ESI†). The deviation from experimental data is of systematic character and can be greatly reduced by the use of functional and basis set dependent scaling factors.[56,57] In terms of the shift of the ν_{COOH} band, the hydrogen bonding needs to be accounted for properly. Many studies have evaluated the performance of DFT functionals with respect to hydrogen bonding (*e.g.* ref. 55 and 58–61) with varying conclusions, as to which functional is "best", although most of these studies focus on binding energies rather than vibrational frequencies. A general agreement appears to be that the PBE exchange–correlation functional describes hydrogen-bonding interactions reliably, with a tendency for overestimation of binding energies in small water clusters with growing cluster sizes.[59] The two-center Hamiltonian matrix elements of DFTB3 are derived from PBE,[34] hence to assess the influence of the DFTB specific approximations we chose PBE to be our reference. However, to evaluate all aspects of the performance of DFT itself with respect to the choice of functional, basis set truncation or anharmonicity effects are beyond the scope of this work. For a coarse comparison, we also show experimentally measured frequencies for the propionic acid monomer and dimer in Table 1, although a direct comparison between computed harmonic normal modes and experimental fundamental frequencies is not possible. Nevertheless, we note that both PBE and DFTB3/3ob overestimate the shift between the dimer and the monomer by 20 cm^{-1} (Fig. 2). Other pure density and hybrid functionals also show this behavior (see ESI†). A clear improvement is made at the double hybrid functional level with B2PLYP, a functional, which yields both harmonic and anharmonic frequencies in good agreement with experiment and higher-level *ab initio* methods.[62]

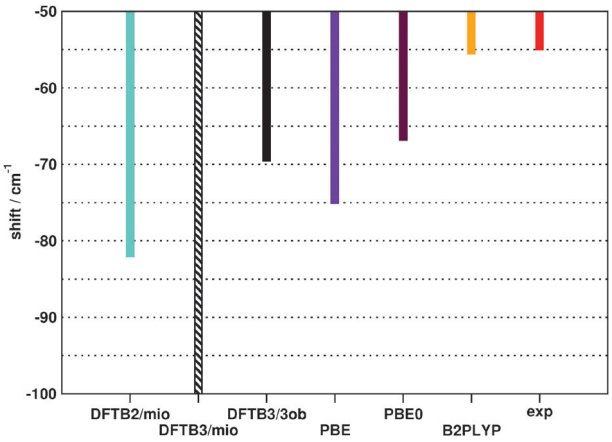

Fig. 2 Shifts of the ν_{COOH} frequencies of the propionic acid dimer with respect to the monomer, computed with DFTB and DFT and compared to experiment.[63]

Table 1 The ν_{COOH} band of hydrogen-bonded clusters of propionic acid and methanol. In models 14 and 15, the strongly dipole-allowed antisymmetric mode is shown. DFT calculations with a def2-TZVP basis set. Numbers given in cm^{-1}. ME = mean error, MAE = mean absolute error, MSE = mean square error

Model	H-bonds	DFTB2/mio	DFTB3/mio	DFTB3/3ob	PBE	PBE0	B2PLYP	Exp.[63]
1	0	1770	1768	1752	1759	1848	1806	1776
2	1	1727	1716	1721	1727			
3		1704	1688	1696	1699			
4		1788	1797	1767	1772			
5		1736	1719	1715	1724			
6	2	1686	1665	1675	1669			
7		1694	1671	1678	1701			
8		1750	1750	1738	1740			
9		1758	1753	1736	1737			
10	3	1652	1621	1639	1639			
11		1702	1684	1685	1679			
12		1714	1700	1702	1703			
13	4	1676	1652	1657	1648			
14		1688	1668	1682	1684	1786	1750	1722
15		1774	1696	1677	1697			
ME w.r.t. PBE		+16	−2	−4				
MAE		17	11	6				
MSE		25	14	9				

In terms of absolute frequencies of the ν_{COOH} band in hydrogen-bonded carboxylic acids (Table 1), the new parametrization improves the performance of DFTB3 significantly, reducing the mean absolute error from 17 cm^{-1} in DFTB2 to just 6 cm^{-1} in DFTB3. The combination of DFTB3 with the mio parameters, as it was used previously for QM/MM geometry optimizations and dynamics simulations, shows a mean absolute error of 11 cm^{-1} and is thus better than DFTB2 and worse than DFTB3/3ob. In the ESI,† we have documented additional tests with the special 3ob parameters for frequencies "3ob-f", which perform inferior to DFTB3/3ob for carboxylic acids. However, for molecules of different chemical character, such as H_2CO, DFTB3/3ob deviates significantly from DFT and experiment, which shows that the performance of semi-empirical methods needs to be evaluated carefully (see ESI† and ref. 34).

For the comparison of FTIR spectra of proteins, the effect of hydrogen bonds on the ν_{COOH} band needs to be described correctly rather than the absolute frequency. It was shown in earlier work that DFTB2 overestimates the effect of hydrogen bonds compared to DFT for strongly hydrogen-bonded systems, such as the acetic acid dimer.[12,33] This effect is even more pronounced for the combination of DFTB3 and the mio parameter set, especially for the propionic acid dimer (model 14). This overestimation with respect to DFT is removed using the new parameter set (Fig. 3). If the propionic acid forms one hydrogen bond, with the OH group as a donor (model 2) or C=O as an acceptor (model 5), the frequency of the ν_{COOH} band is red-shifted by 30 cm^{-1}. Thus, by means of the frequency only, these two situations cannot be distinguished. Model 3 shows a larger red-shift of approximately 60 cm^{-1}, but its configuration corresponds to one hydrogen bond of the hydroxyl group and one distorted interaction with the carbonyl group. If the OH group acts as an acceptor (model 4), ν_{COOH} gets blue-shifted

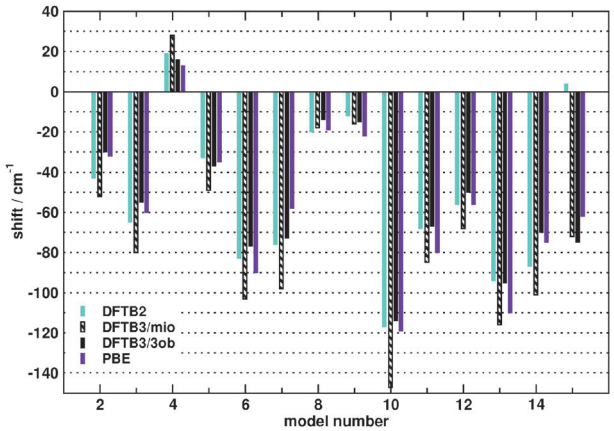

Fig. 3 Shifts of the ν_{COOH} band of propionic acid, due to hydrogen bonds with methanol. Errors for the shifts with respect to PBE (ME/MAE/MSE): DFTB2/mio: +6/12/20, DFTB3/mio: −12/15/19, DFTB3/3ob: +4/8/9.

by 15 cm^{-1}. These results agree well with a similar study on butanoic acid–methanol clusters with hybrid density functional theory.[27]

In addition, we also examined the effect of one hydrogen bond between propionic acid and methanethiol (models 2 to 5 in Fig. 1, with CH_3SH instead of CH_3OH) as a model for the possible interaction between aspartic acid and cysteine in ChR2. Hydrogen bonds involving sulfur are expected to be weaker than those with oxygen, so that the shifts of the ν_{COOH} band due to this hydrogen bond are expected to be smaller. Indeed, DFTB3 describes the shifts due to CH_3SH to be 5 to 10 cm^{-1} smaller than those due to CH_3OH in reasonable agreement with DFT (Fig. 4), although DFTB predicts a greater difference for model 2 between sulfur and oxygen as an acceptor. Note that for sulfur, the 3ob parameters are currently under development, so that we revert to DFTB2/mio and DFTB3/mio for all calculations involving sulfur.

To summarize, DFTB3 in combination with the new 3ob parameter set shows a good agreement with full DFT for the vibrational analysis, both in terms of the absolute frequency, as well as the shifts due to hydrogen bonds for systems like hydrogen-bonded carboxylic acids. We find that in the tested cases, the standard 3ob set performs well, although in other cases, like H_2CO, large deviations from DFT and experiment are observed. The shift of the propionic acid dimer with respect to the monomer, as an example for strong hydrogen bonding, shows that both DFTB and DFT overestimate the experimental shift by 20 cm^{-1}, which gets improved using hybrid or even double hybrid exchange–correlation functionals (see ESI†).

3.2 The C=O stretch vibration in bacteriorhodopsin: dark-adapted *vs.* K states

As a next application, we computed the C=O stretch vibration of D115, both in the dark-adapted state and in the K intermediate, to additionally examine the effect of the environment (electrostatics) on the C=O stretch vibration. In both structures, the OH group of D115 acts as a donor for a hydrogen bond with T90, while it also acts as an acceptor for a hydrogen bond with HOH511, a water molecule, which is resolved in both X-ray structures 1c3w and 1m0k (Fig. 5). The hydrogen-bonding pattern of D115 therefore corresponds to model 8 of the gas-phase clusters (Fig. 1).

In the K intermediate, the retinal has isomerized from all-*trans* to 13-*cis*, while the rest of the protein remains in a conformation very similar to the dark-adapted state. The difference FTIR spectrum of the K intermediate *vs.* the dark-adapted BR shows a symmetric difference band at 1733(+)/1740(−) cm^{-1}, which vanishes for the D115E or D115N mutants.[15] Therefore, this feature has been assigned to a change in the ν_{COOH} band of D115. We examine the ν_{COOH} band with different QM regions. In order to describe the hydrogen-bonded D115 correctly, its hydrogen-bonding partners need to be included in the QM region (D115+T90+WAT, Table 3). If HOH511 is deleted from the structure (D115+T90-WAT), the remaining shift of the ν_{COOH} band is mainly caused by T90. As expected from the model calculation in the gas-phase, the hydrogen bond with T90 red-shifts ν_{COOH} by 30 cm^{-1}. The water molecule blue-shifts the frequency by 10 cm^{-1}. The difference between the QM regions, D115+T90+WAT

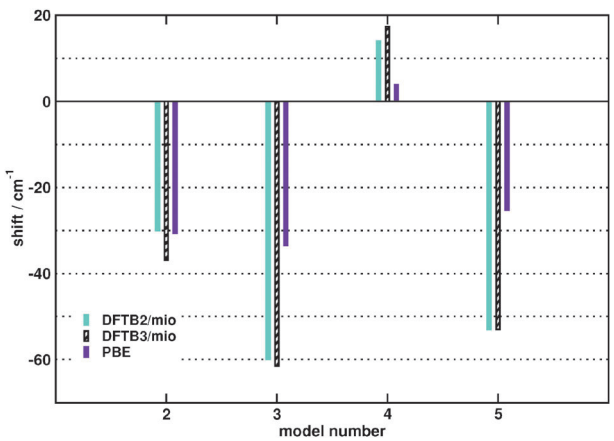

Fig. 4 Shifts of the ν_{COOH} band of propionic acid, due to hydrogen bonds with one CH_3SH molecule (models 2–5 of Fig. 1, with CH_3OH replaced by CH_3SH).

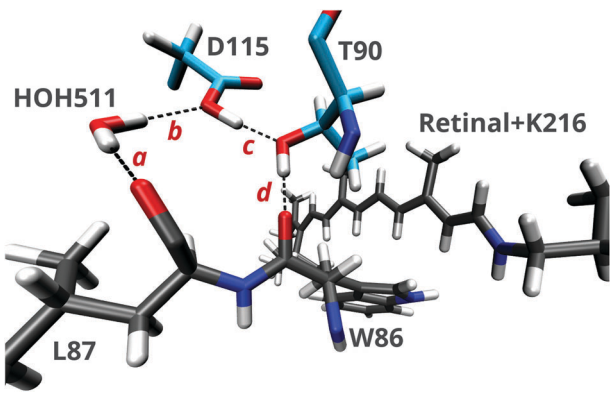

Fig. 5 Hydrogen-bonded network around D115, T90 and water for the QM/MM optimized structure of BR (PDB code: 1c3w). The O–O distances *a*, *b*, *c* and *d* are given in Table 2.

Table 2 O–O distances (in Å) of the hydrogen-bonded network around D115 in the dark-adapted and K states of BR

		O–O distances	
Dist. between	Label in Fig. 5	BR	K
HOH511–L87	*a*	2.80	2.82
HOH511–D115	*b*	2.99	2.93
D115–T90	*c*	2.59	2.61
T90–W86	*d*	2.57	2.57

Table 3 The ν_{COOH} band of D115 in the dark-adapted and K states of BR, computed with DFTB2 and DFTB3. In the QM region D115+T90-WAT, water HOH511 was deleted before structure optimization

		ν_{COOH}/cm^{-1}			
Structure	QM region	Exp.[15]	2/mio	3/mio	3/3ob
BR		1740			
	D115+T90+WAT		1740	1740	1732
	D115+T90		1749	1744	1735
	D115+T90-WAT		1730	1719	1722
	D115		1757	1761	1749
K		1733			
	D115+T90+WAT		1737	1737	1728
	D115+T90		1745	1741	1732
	D115+T90-WAT		1727	1719	1721
	D115		1754	1757	1746

and D115+T90, describes the polarization of the water molecule HOH511, for it is described by DFTB3 in the former and by the TIP3P force field in the latter QM region. This effect is only minor with a shift of 3–4 cm^{-1}.

Only these three residues need to be included in the QM region. The frequencies computed with also K216(+retinal), D212, D85, HOH401, HOH402, HOH406 in the QM region are virtually indistinguishable from the values shown in Table 3, although minor structural differences occur in the Schiff base region of the retinal for the K state. The retinal is more twisted, if described with the CHARMM force field but since the ν_{COOH} band is determined by local effects, the impact of this structural difference is only about ±1 cm^{-1}.

The red-shift of the ν_{COOH} band between the dark-adapted state and the K intermediate is reproduced well with DFTB compared to the experiment. It is interesting to note that both the hydrogen-bonded network of D115 and the C=O bond lengths are very similar in both states. Subtle changes in the O–O distances (Table 2) and the different conformation of the retinal (13-*cis* in K and all-*trans* in the dark-adapted state) are able to cause a shift of 7 cm^{-1}, which is described well with DFTB.

3.3 The C=O stretch vibration of D156 in the DC gate of ChR2

The difference FTIR spectrum between the dark state and the first intermediate P_1 of ChR2 shows a symmetric difference band at 1735(−)/1742(+) cm^{-1}. Compared to the BR/K difference spectrum, the change is opposite in sign and larger in intensity, so that changes other than the hydrogen-bonded network of

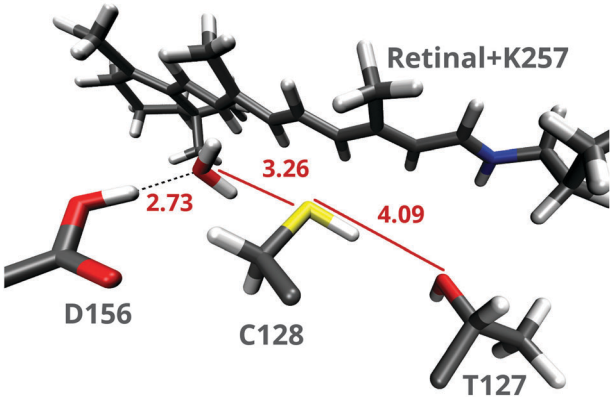

Fig. 6 Hydrogen-bonded network around D156 for a QM/MM optimized structure of ChR2. The O–O and O–S distances are given, respectively (in Å).

D156/C128 may be involved. For the C128T mutant, the difference band pattern is similar to that of BR (1747(−)/1740(+) cm^{-1}), but blue-shifted by 7 cm^{-1}, implying a weaker hydrogen bond. Even less is known about the P_1 state than about the dark state, so that any attempt at modeling remains an issue for future studies. Here, we compute the ν_{COOH} bands of a computational model of ChR2,[26] and the C128T mutant based on this model and compare to the experiments. Molecular dynamics simulations and analysis with a 3D reference interaction site model (3D RISM)[26,64] suggested a much larger number of internal water molecules than resolved in the X-ray structure of the ChR1–ChR2 hybrid[25] or BR.[51] The analysis revealed a stable position of one water molecule between C128 and D156, while it is not present in BR and therefore any homology models based on a BR template. In Fig. 6, the structure of the "indirect" model for the DC gate is displayed. D156 is hydrogen-bonded to one water molecule, while the C128 is oriented to the side chain oxygen atom of T127, the S–O distance being 4.09 Å. The computed frequencies for the ν_{COOH} band agree well with the experimental data for ChR2, which shows that the FTIR experiments can be interpreted on an indirect model as well, where D156 is hydrogen-bonded to one water molecule.

In the MD simulations based on our ChR2 homology model, a direct interaction between D156 and C128 was not observed.[26] Instead, the simulations indicate a stable water molecule bridging C128 and D156. Furthermore, the orientation of C128 in the X-ray structure of the ChR1–ChR2 hybrid, on which our homology model is based, is unsuitable for a direct interaction with D156. Therefore, a DC gate that features a direct interaction is not compatible with our homology model.

The C128T mutant looks very similar to the BR dark-adapted state (Fig. 7) without any water molecule between the D156 and the T128. The ν_{COOH} band is shifted to 1747 cm^{-1} in the ground state of ChR2, which is 7 cm^{-1} higher than in BR, implying a weaker hydrogen bond between D156 and T128. In BR, the position of the water molecule near D115 is well resolved in the X-ray structure,[51] while in C128T, no water molecule was found at this position.[26] Additionally to the model obtained from MD,

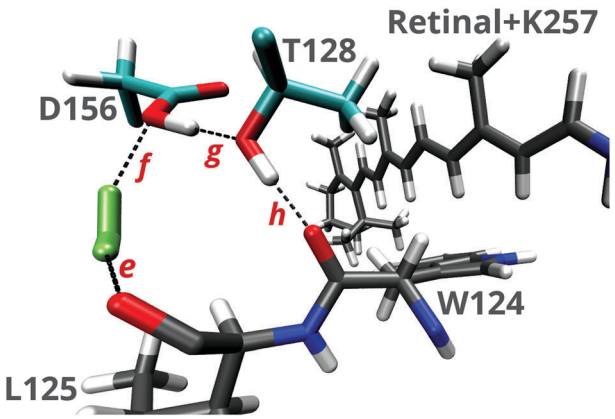

Fig. 7 Hydrogen-bonded network around D156 in the C128T mutant. O–O distances *e*, *f*, *g* and *h* are displayed in Table 5. The water molecule (green) is not present in MD simulations, but inserted manually before structure optimization.

we also built a model with a water molecule near the OH group of D156, similar to BR (shown in green in Fig. 7). However, as the O–O distances are larger compared to those in BR (Table 5), the influence of the water molecule on the ν_{COOH} frequency is smaller (Table 4). The difference between the C=O stretch frequencies between ChR2 and C128T is 12 cm^{-1} as determined by the experiment. Our calculations on the other hand predict similar C=O stretch frequencies for ChR2 and its mutant. One reason behind this deviation is based on the setup of the structure for the mutant. We started from an optimized ChR2 structure, changed the cysteine to threonine and optimized again. Therefore, the structural relaxation is only local. Clearly, extended MD simulations would lead to a better representative structure of the C128T mutant, however, this is beyond the scope of this work.

Clearly, the calculated vibrational frequencies of D156 in ChR2 deviate more from the FTIR experiments, than in BR, where the structural uncertainty is very low. It cannot be expected that our homology model of ChR2,[26] which is based on the X-ray structure of the ChR1–ChR2 hybrid and refined by MD simulations, possesses the same structural certainty as the X-ray structures. The example of BR/K shows that small changes, like subtle conformation changes, minor deviations in the hydrogen-bonding network or a different configuration of the chromophore, lead to shifts of the ν_{COOH} band of 7 cm^{-1}. The major effect, which is the shift of the ν_{COOH} band of 1779 cm^{-1} (gas phase) to 1740 cm^{-1} as in the protein, is dominated by local effects, which are described well with DFTB in the QM/MM framework.

Table 4 The ν_{COOH} band of D156 in the wild type ChR2 and in the C128T mutant computed with DFTB (3ob parameters for S are currently under development)

		ν_{COOH}/cm^{-1}			
Structure	QM region	Exp.[24]	2/mio	3/mio	3/ob
ChR2		1735			
	D156+C128+WAT		1740	1742	—
C128T		1747			
	D156+T128		1738	1733	1735
	D156+T128+WAT		1743	1733	1737

Table 5 O–O distances (in Å) of the hydrogen-bonded network around D156 in the C128T mutant of BR

Dist. between	Label in Fig. 5	O–O distances
WAT–L125	*e*	2.94
WAT–D156	*f*	3.08
D156–T128	*g*	2.66
T128–W124	*h*	2.64

4 Conclusions

By combining DFTB3 with the 3ob parameter set, we showed that it surpasses the accuracy of previously used DFTB versions for the vibrational analysis of carboxylic acids, with a mean absolute error of 6 cm^{-1} with respect to PBE for the frequencies of the ν_{COOH} band, and 7 cm^{-1} for the shifts due to hydrogen-bonding interaction with CH_3OH. Nevertheless, our calculations also showed that the performance of the parametrization depends very much on the type of molecule and vibration to be considered. While the C=O stretch vibration in propionic acid is computed to be 24 cm^{-1} below the experimental value, in an excellent agreement with PBE, in formaldehyde, DFTB3/3ob yields a vibrational frequency that is almost 100 cm^{-1} above the experiment and 80 cm^{-1} above PBE (see ESI†). This example serves as a reminder that the universal performance of semi-empirical methods cannot be guaranteed and has to be analyzed critically in each case.

We studied the FTIR difference spectrum between the dark-adapted state and the K intermediate of BR to show that subtle changes in the hydrogen-bonding network of D115 are able to cause a red-shift of the ν_{COOH} band of 7 cm^{-1}. As an approximative method, it is not the aim of DFTB to seek a quantitative agreement, but rather to recover the effects of the two different structures on the ν_{COOH} frequency, which it does well.

Unfortunately, the availability of "good" models for the channelrhodopsins lagged behind the availability of experimental data for a long time, since models based on X-ray crystallographic experiments and MD simulations only appeared recently. Previously, experimental data have been interpreted often on the basis of homology models, which may or may not be suitable, depending on the choice of template and structural refinement. The DC gate in ChR2 is a structural motif, which is involved in the kinetics of the ion channel. Replacements of either D156 or C128 significantly prolong the open state. Changes in the structure of the DC gate are visible in the FTIR difference spectrum which has been interpreted based on homology to other familiar microbial rhodopsins, such as bacteriorhodopsin. Accordingly, a direct hydrogen bond between the thiol group of C128 and the carbonyl group of D156 has been postulated. However, a direct model for the DC gate is inconsistent with both X-ray crystallographic and FTIR experiments. We have shown that an indirect model, where D156 and C128 interact *via* a water

molecule, can explain the FTIR experiments and additionally is consistent with the X-ray structure of the ChR1–ChR2 hybrid. The vibrational analysis of D156 based on our computational model shows a general agreement with the experimental data, with remaining uncertainties, due to our ChR2 model. The local environment of D156 is described well by this model, leading to a ν_{COOH} frequency of 1740 cm^{-1}, while further structural refinements can lead to changes of the order of 10 cm^{-1}, as it is the case in the difference spectrum of BR/K.

For future studies, it would be interesting to compare the ChR1–ChR2 hybrid in both computations and experiments, since the structure is already known. Clearly, a vibrational analysis of the P_1 intermediate of ChR2 is desirable to obtain further insight into the DC gate structure and its implications on the kinetics of the ion channel. Modeling the P_1 state is ongoing research in our group, since no structural model is available at present, so that its vibrational analysis will be a topic of future studies.

Acknowledgements

This work was supported by the Deutsche Forschungsgemeinschaft FOR1279, ''Protein-based Photoswitches''. Computations were performed in parts at the Steinbruch Centre for Computing of the Karlsruhe Institute of Technology. K.W. gratefully acknowledges help from W. Hujo in answering DFT related questions.

References

1 J. Heberle, *Biochim. Biophys. Acta*, 2000, **1458**, 135–147.
2 R. Vogel and F. Siebert, *Curr. Opin. Chem. Biol.*, 2000, **4**, 518–523.
3 C. Kötting and K. Gerwert, *ChemPhysChem*, 2005, **6**, 881–888.
4 A. Barth, *Prog. Biophys. Mol. Biol.*, 2000, **74**, 141–173.
5 A. Dioumaev, *Biochemistry*, 2001, **66**, 1269–1276.
6 A. K. Dioumaev and M. S. Braiman, *J. Am. Chem. Soc.*, 1995, **117**, 10572–10574.
7 R. Lozier, R. Bogomolni and W. Stoeckenius, *Biophys. J.*, 1975, **15**, 955–962.
8 B. Schobert, J. Cupp-Vickery, V. Hornak, S. O. Smith and J. K. Lanyi, *J. Mol. Biol.*, 2002, **321**, 715–726.
9 A.-N. Bondar, M. Elstner, S. Suhai, J. C. Smith and S. Fischer, *Structure*, 2004, **12**, 1281–1288.
10 A. N. Bondar, J. C. Smith and S. K. Fischer, *Phase Transitions*, 2005, **78**, 671–675.
11 A.-N. Bondar, J. C. Smith and M. Elstner, *Theor. Chem. Acc.*, 2010, **125**, 353–363.
12 P. Phatak, N. Ghosh, H. Yu, Q. Cui and M. Elstner, *Proc. Natl. Acad. Sci. U. S. A.*, 2008, **105**, 19672–19677.
13 P. Phatak, J. S. Frähmcke, M. Wanko, M. Hoffmann, P. Strodel, J. C. Smith, S. Suhai, A.-N. Bondar and M. Elstner, *J. Am. Chem. Soc.*, 2009, **131**, 7064–7078.
14 K. Welke, J. S. Frähmcke, H. C. Watanabe, P. Hegemann and M. Elstner, *J. Phys. Chem. B*, 2011, **115**, 15119–15128.
15 M. S. Braiman, T. Mogi, T. Marti, L. J. Stern, H. G. Khorana and K. J. Rothschild, *Biochemistry*, 1988, **27**, 8516–8520.
16 G. Nagel, T. Szellas, W. Huhn, S. Kateriya, N. Adeishvili, P. Berthold, D. Ollig, P. Hegemann and E. Bamberg, *Proc. Natl. Acad. Sci. U. S. A.*, 2003, **100**, 13940–13945.
17 E. S. Boyden, F. Zhang, E. Bamberg, G. Nagel and K. Deisseroth, *Nat. Neurosci.*, 2005, **8**, 1263–1268.
18 O. Yizhar, L. E. Fenno, M. Prigge, F. Schneider, T. J. Davidson, D. J. O'Shea, V. S. Sohal, I. Goshen, J. Finkelstein, J. T. Paz, K. Stehfest, R. Fudim, C. Ramakrishnan, J. R. Huguenard, P. Hegemann and K. Deisseroth, *Nature*, 2011, **477**, 171–178.
19 K. Deisseroth, *Nat. Methods*, 2011, **8**, 26–29.
20 E. Ritter, K. Stehfest, A. Berndt, P. Hegemann and F. J. Bartl, *J. Biol. Chem.*, 2008, **283**, 35033–35041.
21 A. Berndt, O. Yizhar, L. A. Gunaydin, P. Hegemann and K. Deisseroth, *Nat. Neurosci.*, 2009, **12**, 229–234.
22 I. Radu, C. Bamann, M. Nack, G. Nagel and E. Bamberg, *J. Am. Chem. Soc.*, 2009, **131**, 7313–7319.
23 C. Bamann, R. Gueta, S. Kleinlogel, G. Nagel and E. Bamberg, *Biochemistry*, 2010, **49**, 267–278.
24 M. Nack, I. Radu, M. Gossing, C. Bamann, E. Bamberg, G. F. von Mollard and J. Heberle, *Photochem. Photobiol. Sci.*, 2010, **9**, 194–198.
25 H. Kato, F. Zhang, O. Yizhar, C. Ramakrishnan, T. Nishizawa, K. Hirata, J. Ito, Y. Aita, T. Tsukazaki, S. Hayashi, P. Hegemann, A. Maturana, R. Ishitani, K. Deisseroth and O. Nureki, *Nature*, 2012, **482**, 369–374.
26 H. C. Watanabe, K. Welke, D. J. Sindhikara, P. Hegemann and M. Elstner, *J. Mol. Biol.*, 2013, DOI: 10.1016/j.jmb.2013.01.033.
27 B. Nie, J. Stutzman and A. Xie, *Biophys. J.*, 2005, **88**, 2833–2847.
28 H. C. Watanabe, K. Welke, F. Schneider, S. Tsunoda, F. Zhang, K. Deisseroth, P. Hegemann and M. Elstner, *J. Biol. Chem.*, 2012, **287**, 7456–7466.
29 M. Elstner, D. Porezag, G. Jungnickel, J. Elsner, M. Haugk, T. Frauenheim, S. Suhai and G. Seifert, *Phys. Rev. B: Condens. Matter Mater. Phys.*, 1998, **58**, 7260–7268.
30 Y. Yang, H. Yu, D. York, Q. Cui and M. Elstner, *J. Phys. Chem. A*, 2007, **111**, 10861–10873.
31 M. Gaus, Q. Cui and M. Elstner, *J. Chem. Theory Comput.*, 2011, **7**, 931–948.
32 H. Yu and Q. Cui, *J. Chem. Phys.*, 2007, **127**, 234504.
33 J. S. Frähmcke, M. Wanko, P. Phatak, M. A. Mroginski and M. Elstner, *J. Phys. Chem. B*, 2010, **114**, 11338–11352.
34 M. Gaus, A. Goez and M. Elstner, *J. Chem. Theory Comput.*, 2013, **9**, 338–354.
35 M. D. Hanwell, D. E. Curtis, D. C. Lonie, T. Vandermeersch, E. Zurek and G. R. Hutchison, *J. Cheminf.*, 2012, **4**, 17.
36 F. Neese, *ORCA – An ab initio*, density functional and semiempirical program package, Version 2.9, Max Planck Institute for Bioinorganic Chemistry, Muelheim, Germany, 2012.
37 J. P. Perdew, K. Burke and M. Ernzerhof, *Phys. Rev. Lett.*, 1996, **77**, 3865–3868.
38 F. Weigend and R. Ahlrichs, *Phys. Chem. Chem. Phys.*, 2005, **7**, 3297–3305.

39 F. Weigend, *Phys. Chem. Chem. Phys.*, 2006, **8**, 1057–1065.
40 C. Adamo and V. Barone, *J. Chem. Phys.*, 1999, **110**, 6158–6170.
41 F. Neese, F. Wennmohs, A. Hansen and U. Becker, *Chem. Phys.*, 2009, **356**, 98–109.
42 F. Weigend, *J. Comput. Chem.*, 2008, **29**, 167–175.
43 S. Grimme, *J. Chem. Phys.*, 2006, **124**, 034108.
44 O. Vahtras, J. Almlöf and M. Feyereisen, *Chem. Phys. Lett.*, 1993, **213**, 514–518.
45 F. Weigend and M. Häser, *Theor. Chem. Acc.*, 1997, **97**, 331–340.
46 A. Hellweg, C. Hättig, S. Höfener and W. Klopper, *Theor. Chem. Acc.*, 2007, **117**, 587–597.
47 Q. Cui, M. Elstner, E. Kaxiras, T. Frauenheim and M. Karplus, *J. Phys. Chem. B*, 2001, **105**, 569–585.
48 B. R. Brooks, C. L. Brooks III, A. D. Mackerell Jr., L. Nilsson, R. J. Petrella, B. Roux, Y. Won, G. Archontis, C. Bartels, S. Boresch, A. Caflisch, L. Caves, Q. Cui, A. R. Dinner, M. Feig, S. Fischer, J. Gao, M. Hodoscek, W. Im, K. Kuczera, T. Lazaridis, J. Ma, V. Ovchinnikov, E. Paci, R. W. Pastor, C. B. Post, J. Z. Pu, M. Schaefer, B. Tidor, R. M. Venable, H. L. Woodcock, X. Wu, W. Yang, D. M. York and M. Karplus, *J. Comput. Chem.*, 2009, **30**, 1545–1614.
49 A. D. MacKerell Jr., D. Bashford, M. Bellott, R. L. Dunbrack Jr., J. D. Evanseck, M. J. Field, S. Fischer, J. Gao, H. Guo, S. Ha, D. Joseph-McCarthy, L. Kuchnir, K. Kuczera, F. T. K. Lau, C. Mattos, S. Michnick, T. Ngo, D. T. Nguyen, B. Prodhom, W. E. Reiher, B. Roux, M. Schlenkrich, J. C. Smith, R. Stote, J. Straub, M. Watanabe, J. Wiórkiewicz-Kuczera, D. Yin and M. Karplus, *J. Phys. Chem. B*, 1998, **102**, 3586–3616.
50 A. D. Mackerell Jr., M. Feig and C. L. Brooks III, *J. Comput. Chem.*, 2004, **25**, 1400–1415.
51 H. Luecke, B. Schobert, H.-T. Richter, J.-P. Cartailler and J. K. Lanyi, *J. Mol. Biol.*, 1999, **291**, 899–911.
52 J. Sasaki, J. K. Lanyi, R. Needleman, T. Yoshizawa and A. Maeda, *Biochemistry*, 1994, **33**, 3178–3184.
53 L. S. Brown, J. Sasaki, H. Kandori, A. Maeda, R. Needleman and J. K. Lanyi, *J. Biol. Chem.*, 1995, **270**, 27122–27126.
54 P. H. König, M. Hoffmann and T. Frauenheim, *J. Phys. Chem. B*, 2005, **109**, 9082–9095.
55 K. E. Riley, B. T. Op't Holt and K. M. Merz, *J. Chem. Theory Comput.*, 2007, **3**, 407–433.
56 J. P. Merrick, D. Moran and L. Radom, *J. Phys. Chem. A*, 2007, **111**, 11683–11700.
57 M. L. Laury, M. J. Carlson and A. K. Wilson, *J. Comput. Chem.*, 2012, **33**, 2380–2387.
58 J. Ireta, J. Neugebauer and M. Scheffler, *J. Phys. Chem. A*, 2004, **108**, 5692–5698.
59 B. Santra, A. Michaelides and M. Scheffler, *J. Chem. Phys.*, 2007, **127**, 184104.
60 Y. Zhao and D. G. Truhlar, *J. Chem. Theory Comput.*, 2007, **3**, 289–300.
61 L. Goerigk and S. Grimme, *Phys. Chem. Chem. Phys.*, 2011, **13**, 6670–6688.
62 M. Biczysko, P. Panek, G. Scalmani, J. Bloino and V. Barone, *J. Chem. Theory Comput.*, 2010, **6**, 2115–2125.
63 W. Sander and M. Gantenberg, *Spectrochim. Acta, Part A*, 2005, **62**, 902–909.
64 D. J. Sindhikara, N. Yoshida and F. Hirata, *J. Comput. Chem.*, 2012, **33**, 1536–1543.